Measurement of blood oxygen saturation using a single wavelength photoacoustic Z-scan technique

Albert Kamanzi[1†], Helena Rudolph[2], Sumit Agrawal[2],
Sri Rajasekhar Kothapalli[2,3] and Chandra S Yelleswarapu[1]

[1]Department of Physics, University of Massachusetts Boston, 100 Morrissey Blvd, Boston, MA 02125, USA

[2]Department of Biomedical Engineering, The Pennsylvania State University, University Park, PA 16802, USA

[3]Penn State Cancer institute, The Pennsylvania State University, Hershey, PA 17033, USA.

This article is dedicated to Prof DVGLN Rao

Measuring and monitoring oxygen saturation (SO2) levels in the blood is very important in medicine. Low oxygen levels in the blood is an early warning sign for immediate medical care as it can be related to a wide variety of chronic illnesses, including viral infections. Also, mapping of SO2 values by performing a raster scan across the region of interest *in vivo* is essential in clinical and research settings, such as evaluating the therapeutic effects of treatment and monitoring wound healing. Conveniently, the two main derivatives of hemoglobin, oxyhemoglobin and deoxyhemoglobin, work as strong natural optical contrast agents with distinct spectral profiles. The differential optical absorption of oxy- and deoxy hemoglobins has been exploited by non-invasive optical sensing methods, such as pulse oximetry, to quantify blood SO2 levels. However, the accuracy of conventional optical methods is affected by skin color and strong optical scattering of biological tissue. Overcoming the optical scattering limits, photoacoustic imaging has shown great promise in mapping deep tissue SO2 levels. However, bulky and multiwavelength lasers are used in conventional photoacoustic imaging, limiting the portability, affordability and widespread use of the technology. In this work, we quantify the blood oxygen saturation by measuring the nonlinear absorption coefficient (β) of blood samples using a single wavelength photoacoustic Z-scan (PAZ) technique. Results demonstrate a linear dependency between β and blood SO2 levels. In future the PAZ scan could pave the way for many *in vivo* biomedical applications. © Anita Publications. All rights reserved.

Keywords: Blood oxygenation, Z-scan technique, Photoacoustics, Nonlinear optical studies of blood.

1 Introduction

Adequate oxygen is critical for all normal physiological functions of living subjects. In humans, oxygen is carried from lungs to the rest of the body by hemoglobin molecule, an iron containing protein found in red blood cells. The "heme" in hemoglobin is responsible for binding oxygen molecules. When all the four available bonding sites of the hemoglobin are occupied by oxygen molecules then it is referred to as saturated or oxyhemoglobin (HbO_2), and is bright red in color. The oxygen-unloaded hemoglobin is called deoxyhemoglobin (Hb) and is purple-blue in color. Blood oxygen saturation (SO2), defined as the ratio of HbO_2/HbT (where HbT = HbO_2 + Hb is the total hemoglobin concentration), is one of the standard vital signs measured in medicine along with temperature, pulse rate, and blood pressure. Constant monitoring of blood oxygenation levels has become very important in medicine [1], especially for the management of many life-threatening illnesses such as cancer, pneumonia (lung infection), severe traumatic brain injury, ischemia, sepsis, and shock [2-9]. Monitoring the flow of blood and tracking the changes in oxygenation levels has

Corresponding authors

e mail: *Chandra.yelleswarapu@umb.edu* (Chandra S); *szk416@psu.edu* (Sri Rajasekhar Kothapalli).

[†]*This article is the part of the author's M.S thesis*

also become an important tool for *in vivo* functional imaging [10-19]. In addition, constant monitoring of blood SO2 levels of patients has become routine in intensive care units. In the recent Covid-19 outbreak, 75% of Covid patients suffered from induced pneumonia [20,21]. For pneumonia patients, formation of pus-like fluid lowers the lung capacity, causing difficulty in oxygen absorption and decrease of SO2 level. Pulse oximeters are commonly used for measuring peripheral SO2 level of a finger. To quantify SO2, these oximeters utilize two LED illuminations in the tissue transparent window, one at 660 nm wavelength and another one at 940 nm (near-infrared) wavelength. As shown in Fig 1, Hb and HbO_2 have distinct spectral characteristics in the VIS-NIR region, with a standard cross over at the isosbestic wavelengths of around 550, 580 and 800 nm, where both the hemoglobins have the same optical absorbance [22]. In particular, HbO_2 absorbs more near-infrared light (940 nm) compared to red light (660 nm), whereas Hb absorbs more 660 nm light in reference to 940 nm. This differential optical absorption is exploited to quantify SO2 level. However, recent data on Covid-19 patients suggests that pulse oximeters provide less accurate SO2 level in people with skin color (non-white) [23]. Several alternative techniques have been developed to estimate the amount of oxygen in blood such as resonance Raman intravital microscopy [24], coherent anti-Stokes Raman scattering [25], spectroscopic spectral-domain optical coherence tomography [26], and magnetic resonance imaging (MRI) [27]. While optical techniques suffer from dominant optical scattering and thereby limit their accuracy in deep tissue, functional MRI measurements of SO2 (based on difference in the paramagnetic properties of HbO_2 and Hb) are rather indirect and often leading to false positive rates [28].

In contrast, the emerging hybrid optical excitation and acoustic detection technique called photoacoustic (PA) imaging has been demonstrated to provide reliable SO2 measurements in clinical applications of breast cancer detection, monitoring Chron's disease activity, and assessing tissue metabolism [29-32]. The difference in spectral characteristics of Hb and HbO_2 are exploited in PA spectroscopy and *in vivo* PA imaging, However, the conventional PA imaging technologies use multiwavelength lasers that are often bulky and high cost. Therefore, a simple, portable, and affordable PA imaging or sensing technology capable of accurately estimating peripheral SO2 level is desired. In this study, we demonstrate the feasibility of our previously reported nonlinear photoacoustic Z-scan (PAZ) technique [33] to quantitatively characterize the blood oxygenation using a single wavelength. The obtained nonlinear absorption coefficient (β) values for oxy- and deoxy- hemoglobins show a linear dependency against oxygen level in the blood.

2 Experimental details

2.1 Blood sample preparation

A protocol was developed to prepare oxygenating and deoxygenating blood samples. 1 ml of Lysed sheep blood, purchased from Quad Fife (Ryegate, Montana), was placed in a Ziploc bag and then inflated with oxygen to obtain HbO_2, and carbon dioxide or argon to obtain Hb. The bags were then placed on a rocker (Benchmark Scientific Ultracruz 2D rocker) to achieve maximum mixing efficiency. The duration of time required to attain optimum HbO_2 and/or Hb is about 2 hours. Shorter time periods caused less oxygenation and deoxygenation of samples while longer periods resulted in bags getting deflated and water evaporation from the bags. After 2 hour inflation time, the oxy- and deoxy- blood samples have visibly stark contrasting colors; deoxyhemoglobin sample being much darker than the oxyhemoglobin. The blood was pipetted out from the bags by opening the ziploc bags as little as possible. The samples were then placed into the cuvettes and filled to the top. This process had to be done fast, particularly for the deoxy samples to minimize the contact with air. The cuvettes were then closed with tops, allowing for some of the samples to overflow ensuring no air is left inside. The samples were then sealed using the parafilm wrap around the contact of the cuvette and the top. The best oxy- and deoxy- blood samples obtained had hemoglobin oxygen saturation values of 92% and 14%, respectively.
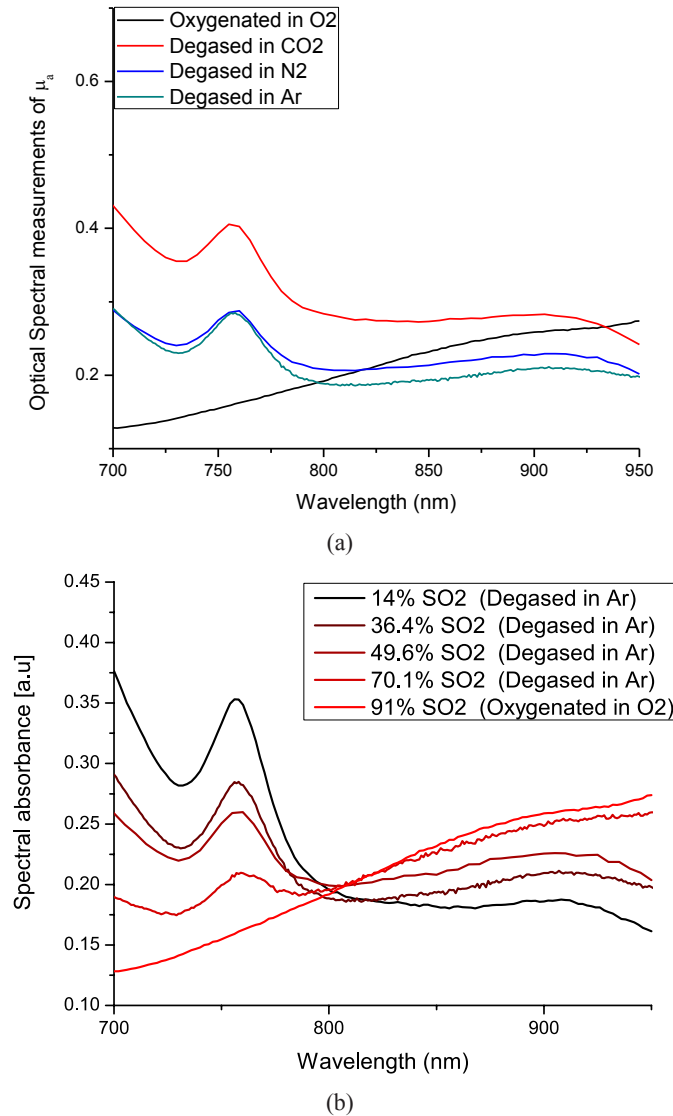
(a)

(b)

Fig 1. (a) comparison of absorption spectra of blood degassed with various gases.
(b) Absorption spectra showing various oxygen saturation levels (Hb to HbO$_2$)
obtained by degassing blood with oxygen and argon.

2.2 Oxygen saturation measurement

The VIS-NIR spectra of the prepared HbO$_2$ and Hb samples, Fig 1, were obtained using Agilent Cary 60 UV-VIS spectrometer. Obtaining the standard isosbestic wavelength at 800 nm for the prepared Hb and HbO$_2$ samples proved challenging. We found that it is not possible to achieve 100% oxygenated or and deoxygenated hemoglobin as blood becomes degassed as soon as it gets in contact with the atmospheric air. For preparing HbO$_2$, pure oxygen gas seemed to be the best choice. For Hb, when carbon dioxide is used, the isosbestic wavelength was observed at ~ 930 nm instead of 800 nm, as shown in Fig 1(a). This could be attributed to the fact that the carbon dioxide has an additional effect of making the blood samples more acidic. However, when argon gas was used to prepare Hb samples, the standard isosbestic wavelength of

800 nm was obtained (Fig 1(b)). We also tested mixing blood with nitrogen gas, and the result showed that the isosbestic crossover (830 nm) was better than the CO_2 case. Once a satisfactory degassing method was achieved, several samples with various oxygenation levels were prepared and their SO2 values, depicted in inset of Fig (b), were estimated using a Matlab routine.

The absorption coefficient of blood can be expressed as:

$$\mu_a = \sigma_{Hb} N_{Hb} + \sigma_{HbO_2} N_{HbO_2}$$

where, σ_{HbR} and σ_{HbO_2} are the spectral absorption cross sections of deoxy-hemoglobin (Hb) and oxy-hemoglobin (HbO_2), respectively. N_{Hb} and N_{HbO2} are the number of Hb and HbO_2 absorbers per unit volume. Taking two measurements on either side of the isosbestic wavelength, and using least squares fitting methods, it is possible to measure the oxygenation level in blood. A Matlab program was developed to estimate the SO2 value using the absorbance obtained from UV-VIS spectra. Inputs for the program are absorption coefficients (m_a, mm^{-1}) and the corresponding wavelengths (nm) λ_1 and λ_2, which are optimally chosen to be on either of the isosbestic point. The first matrix on the right-hand side contains the absorption cross sections of oxy- and deoxy- hemoglobins. Using the absorption cross section values from literature, [22,34,35], we calculated the SO2 values for the prepared Hb and HbO_2 samples.

$$\begin{bmatrix} \mu(\lambda_1) \\ \mu(\lambda_1) \end{bmatrix} = \begin{bmatrix} \sigma_{HbO_2}(\lambda_1)\ \sigma_{Hb}(\lambda_1) \\ \sigma_{HbO_2}(\lambda_2)\ \sigma_{Hb}(\lambda_2) \end{bmatrix} \begin{bmatrix} N_{HbO_2} \\ N_{Hb} \end{bmatrix}$$
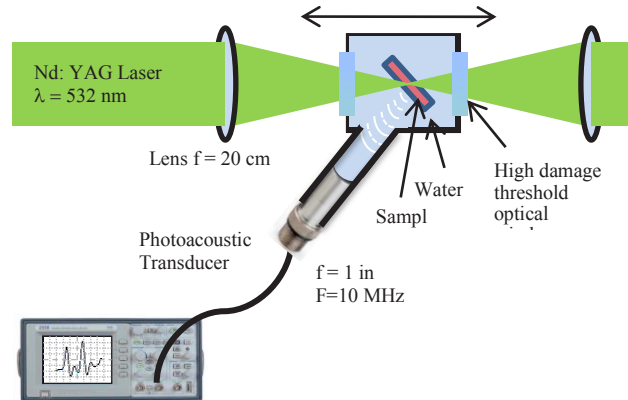
2.3 Photoacoustic Z-scan

Fig 2. Schematic of the PAZ-scan setup – 532 nm nanosecond laser beam is focused onto the sample using a 20 cm converging lens. As the sample is translated through focal zone, the generated acoustic waves are detected using a focused ultrasound transducer.

In year 2010, we demonstrated a novel PAZ-scan technique in which the generated nonlinear photoacoustic behavior is used to measure the third-order nonlinear optical (NLO) absorption coefficients for saturable and reverse saturable absorption materials [33]. Since then, we applied this technique to study the NLO properties of a variety of materials [36-38]. PAZ-scan combines the advantages offered by the conventional optical Z-scan technique [39] and optical absorption based high sensitive photoacoustic detection. To perform the PAZ-scan experiments, a Nd: YAG laser (Continuum Minilite II, λ_{exc} = 532 nm, pulse width τ_p = 3 ns, Pulse rep rate is 10 Hz, 100 µJ/pulse) was used. Schematic of the experimental setup is shown in Fig 2. The 2 mm cuvette sample holder is mounted in a custom-made cell that contains water for ultrasound coupling. The sample cell was placed at 45° with respect to the incident laser beam, because of which, the optical path length L = 2.83 mm. As the laser pulse is incident on the sample, most of the optical

energy is absorbed by the sample which is converted into heat. Heat production by the excited molecules produces pressure transients and thus wideband ultrasonic emission in its local environment. The generated ultrasonic waves (PA signal) are then detected using a 10 MHz focused water immersion transducer (Olympus NDT U8423240). The sample holder is mounted on a XYZ translation stage and aligned carefully so that the PA signal collected by the transducer is optimum. The sample holder is then translated along the direction of the laser beam in discrete steps such that the sample is scanned through the complete focal zone (on either side of the focal point) of the beam along the Z-direction. The beam waist is about 65 µm, and the Rayleigh range is ~2.5 cm. The recorded photoacoustic signals measurements for each step along the focal zone are then plotted and fitted on the nonlinear Eq (3) and the best fitting nonlinear absorption coefficient (β) values are obtained.

3 Result and Discussion

The plots shown in Fig 3 represent the PAZ-scan curves for three different blood samples. The x-axis shows positions of the sample along the light propagating Z-axis, while the y-axis displays normalized photoacoustic signal values. Assuming a linear absorption in the far field, that is 7 cm away from the focus of the beam, we used the corresponding PA signal at this far field location to normalize the PA data. Then the data is fitted to third-order nonlinear absorption equation [33,35]:

$$p_{norm}(z) = 1 + \frac{\beta}{\alpha} \frac{E}{\pi t \omega_0^2 \left(1 + \left(\frac{z}{z_0}\right)^2\right)^2} \tag{3}$$

where E is the energy of the incident laser beam, α is the linear absorption coefficient, and ω_0 is the beam waist. The best fit β values for all the samples are shown in Table 1. The trend in Fig 4 indicates a linear dependence between β and SO2. However, despite the overall linear trend the error bars in each measurement are too large. Therefore, more measurements are required. Additionally, the linear absorption coefficients values of oxy- and deoxy- hemoglobins are very close at the 532 nm wavelength (see Table below). This limits the maximum range of possible β values. Hence, these experiments need to be performed at wavelengths (say at 700 nm or 1064 nm) where the difference between oxy- and deoxy- hemoglobin extinction coefficients is large.

Table 1. Results from nonlinear fitting of Z-scan data

SO2 [%]	E (J)	α (m^{-1})	β (m/W)
27.4	1.13E-04	22216	4.19E-08
33.4	1.08E-04	22320.4	4.11E-08
36.1	1.12E-04	22367.7	4.28E-08
60.9	1.08E-04	22806.4	4.52E-08
70.3	1.09E-04	22971.6	4.55E-08
77.6	1.08E-04	23100.6	4.91E-08
89.4	1.05E-04	23308.7	4.74E-08
87.3	1.07E-04	23260.4	4.92E-08
92.1	1.02E-04	23361.5	4.93E-08

5 Conclusions

A method for consistently obtaining oxygenated and deoxygenated blood samples was developed. Obtaining deoxygenated blood samples was more challenging, because of the high affinity for oxygen in

the air to bind to the hemoglobin molecules. Optimum conditions for degassing blood samples were found. Using the linear least squares fitting method for calculating oxygen saturation level, a Matlab function was written and used to characterize samples. Nonlinear optical absorption coefficients of blood samples with
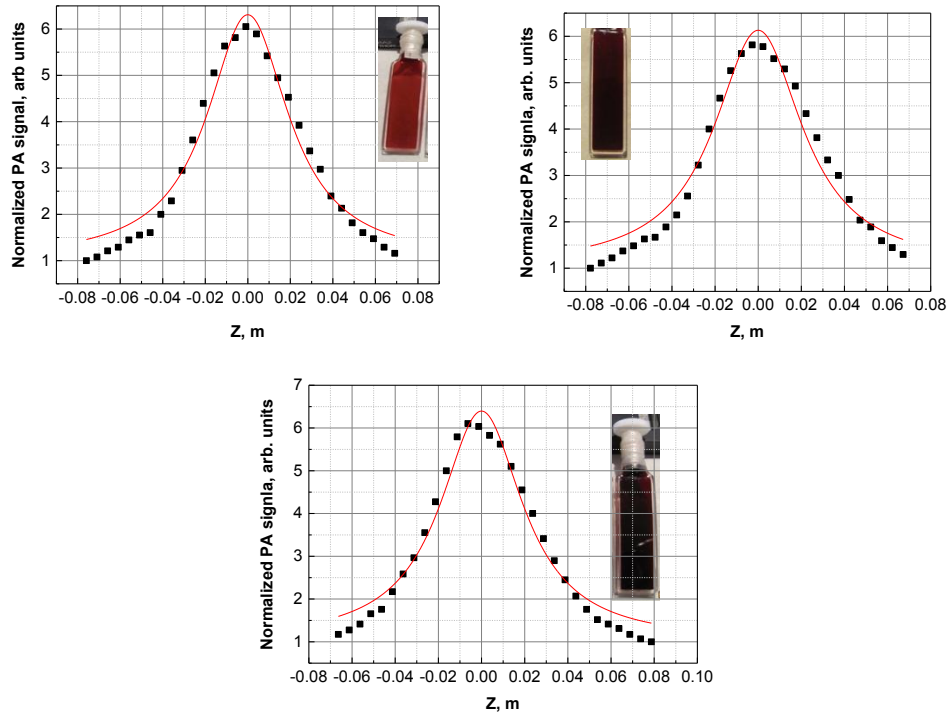

Fig 3. PAZ-scan fitting for three different blood samples with oxygenation (SO2) of (a) 89%, (b) 60%, and (c) 27%. X-axis represents the position of the sample along the focal zone; Z = 0 is the focal point. Y-axis is normalized PA signal.
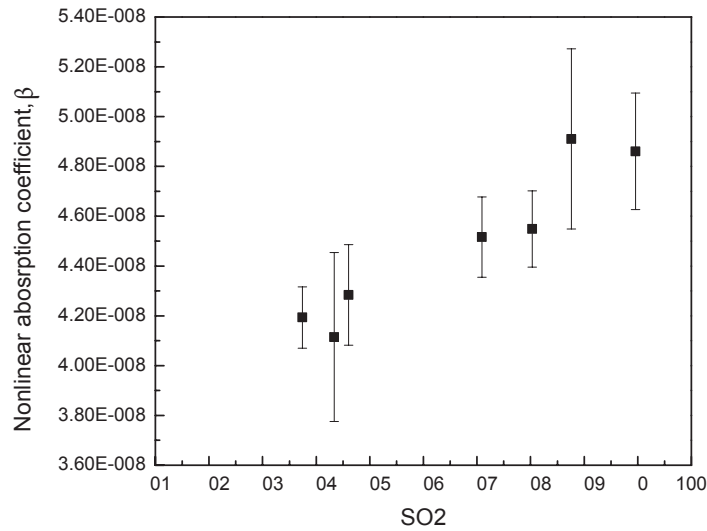

Fig 4. Plot between the nonlinear absorption coefficient β and the SO2 values.

different oxygenation were measured using a photoacoustic Z (PAZ)-scan method performing at a single wavelength (532 nm). Using the data from the SO2 calculations, the nonlinear optical absorption results were shown to change linearly with the varying blood oxygenation levels. Hence, it is possible to obtain the blood oxygen levels from the nonlinear absorption coefficients and eliminate the errors introduced by assuming an entirely linear absorption process. The PAZ-scan also eliminated the need for using two or more wavelengths of estimating blood oxygen saturation. The next step will be to perform the PAZ-scan measurements in the therapeutic window, and specifically at wavelength where the alpha values are different.

Acknowledgements

References

1. Reinhart K, Kuhn H J, Hartog C, Bredle D L, Continuous central venous and pulmonary artery oxygen saturation monitoring in the critically ill, *Intensive Care Med*, 30(2004)1572–1578.
2. Lee M, Assessment of oxidative stress and antioxidant property using electron spin resonance (ESR) spectroscopy, *J Clin Biochem Nutr,* 52(2013)1–8.
3. Blockley N P, Griffeth V E, Simon A B, Buxton R B, A review of calibrated blood oxygenation level-dependent (BOLD) methods for the measurement of task-induced changes in brain oxygen metabolism, *NMR Biomed*, 26(2013)987–1003.
4. Culver J P, Durduran T, Furuya D, Cheung C, Greenberg J H, Yodh A G, Diffuse optical tomography of cerebral blood flow, oxygenation, and metabolism in rat during focal ischemia, *J Cerebral Blood Flow & Metabolism*, 23(2003)911–924.
5. Leyba K A, Vasudevan S, O'Sullivan T D, Goergen C J, Evaluation of Hemodynamics in a Murine Hindlimb Ischemia Model Using Spatial Frequency Domain Imaging, *Lasers Surg Med*, 53(2021)557–566.
6. Roche-Labarbe N, Somatosensory evoked changes in cerebral oxygen consumption measured non-invasively in premature neonates, *Neuroimage*, 85(2014)279–286.
7. Li M, Hu J, Miao Y, Shen H, Tao D, Yang Z, Li Q, Xuan Y S, Raza W, Alzubaidi S, Haacke E M, *In vivo* measurement of oxygenation changes after stroke using susceptibility weighted imaging filtered phase data, *PLoS One*, 8(2013)e63013; doi. doi.org/10.1371/journal.pone.0063013.
8. Das B P, Sharma M, Bansal S, Philip M, Umamaheswara Rao G S, Prognostic value of tissue oxygen monitoring and regional cerebral oxygen saturation monitoring and their correlation in neurological patients with sepsis: a preliminary, prospective, observational study, *J Neurosurg Anesthesiol*, 32(2020)77–81.
9. Chen J, Zhang Y, He L, Liang Y, Wang L, Wide-field polygon-scanning photoacoustic microscopy of oxygen saturation at 1-MHz A-line rate, *Photoacoustics*, 20(2020)100195; doi. org/10.1016/j.pacs.2020.100195.
10. Agrawal S, Singh M K, Yang X, Albahrani H, Dangi A, Kothapalli S R, Functional, molecular and structural imaging using LED-based photoacoustic and ultrasound imaging system, *Photons Plus Ultrasound: Imaging and Sensing*, 11240(2020)112405A; doi.org/10.1117/12.2547048.
11. Foo S S, Abbott D F, Lawrentschuk N, Scott A M, Functional imaging of intratumoral hypoxia, *Mol* Imaging Biol, 6(2004)291–305.

12. Rebling J, Estrada H, Gottschalk S, Sela G, Zwack M, Wissmeyer G, Ntziachristos V, Razansky D, Dual-wavelength hybrid optoacoustic-ultrasound biomicroscopy for functional imaging of large-scale cerebral vascular networks, *J biophotonic*s, 11(2018)e201800057; doi.org/10.1002/jbio.201800057.

13. Ueda S, Saeki T, Osaki A, Yamane T, Kuji I, Bevacizumab induces acute hypoxia and cancer progression in patients with refractory breast cancer: multimodal functional imaging and multiplex cytokine analysis, *Clin Cancer Res*, 23(2017)5769–5778.

14. Nishiyama K, Ito N, Orita T, Hayashida K, Arimoto H, Beppu S, Abe M, Unoki T, Endo T, Murai A, Hatada T, Regional cerebral oxygen saturation monitoring for predicting interventional outcomes in patients following out-of-hospital cardiac arrest of presumed cardiac cause: a prospective, observational, multicentre study, *Resuscitation*, 96(2015)135–141.

15. Rivers EP, Ander DS, Powell D, Central venous oxygen saturation monitoring in the critically ill patient, *Curr Opin Crit Care*, 7(2001)204–211.

16. Medikonda R, Ong C S, Wadia R, Goswami D, Schwartz J, Wolff L, Hibino N, Vricella L, Barodka V, Steppan J, A review of goal-directed cardiopulmonary bypass management in pediatric cardiac surgery, *World J Pediatr Congenit Heart Surg*, 9(2018)565–572.

17. Kovarova L, Valerianova A, Kmentova T, Lachmanova J, Hladinova Z, Malik J, Low cerebral oxygenation is associated with cognitive impairment in chronic hemodialysis patients, *Nephron*, 139(2018)113–119.

18. Alvarez D, Hornero R, Marcos JV, del Campo F, Multivariate analysis of blood oxygen saturation recordings in obstructive sleep apnea diagnosis, *IEEE Trans Biomed Eng*, 57(2010)2816–2824.

19. Li T, Lin Y, Shang Y, He L, Huang C, Szabunio M, Yu G, Simultaneous measurement of deep tissue blood flow and oxygenation using noncontact diffuse correlation spectroscopy flow-oximeter, *Sci Rep*, 3, 1358(2013); doi.org/10.1038/srep01358.

20. "Pneumonia." World Health Organization. World Health Organization. Accessed March 27, 2020. https://www.who.int/news-room/fact-sheets/detail/pneumonia.

21. Harris M, Clark J, Coote, Fletcher P, Harnden A, McKean M, Thomson A, British Thoracic Society guidelines for the management of community acquired pneumonia in children: update 2011, *Thorax*, 66(2011)ii1-ii23; doi.org/10.1136/thoraxjnl-2011-200598.

22. Jacques S L, Optical properties of biological tissues: a review, *Phys Med Bio*, 58(2013)R37; doi.org/10.1088/0031-9155/58/11/R37.

23. Sjoding M W, Dickson R P, Iwashyna T J, Gay S E, Valley T S, Racial Bias in Pulse Oximetry Measurement, *N Engl J Med*, 383(2020)2477–2478.

24. Tiba M H, Awad A B, Pennington A, Fung C M, Napolitano L M, Park P K, Machado-Aranda D A, Gunnerson K J, Romfh P, Ward K R, Resonance Raman spectroscopy derived tissue hemoglobin oxygen saturation in critically ill and injured patients, *Shock*, 56(2021)92–97.

25. Rinia H, Bonn M, Vartiainen E E, Schaffer C B, Mueller M, Spectroscopic analysis of the oxygenation state of hemoglobin using coherent anti-Stokes Raman scattering, *J Biomed Opt*, 11(2006)0505021; doi.org/10.1117/1.2355671.

26. Poddar R, Basu M, Characterization and oxygen saturation study of human retinal blood vessels evaluated by spectroscopic optical coherence tomography angiography, *Opt Laser Technol*, 122(2020):1058861; doi.org/10.1016/j.optlastec.2019.105886.

27. O'Connor J P, Robinson S P, Waterton J C. Imaging tumour hypoxia with oxygen-enhanced MRI and BOLD MRI, *Brit J Radiol*, 92(2019)201806421-12; doi.org/10.1259/bjr.20180642.

28. Eklund A, Nichols TE, Knutsson H, Cluster failure: why fMRI inferences for spatial extent have inflated false-positive rates, *Proc Natl Acad Sci.* (*U.S.A*), 113(2016)7900–7905.

29. Bok T, Hysi E, Kolios M C, In vivo photoacoustic assessment of the oxygen saturation changes in the human radial artery: a preliminary study associated with age, *J Biomed Opt*, 26(2021)036006; doi.org/10.1117/1.JBO.26.3.036006.

30. Lin L, Hu P, Shi J, Appleton C M, Maslov K, Li L, Zhang R, Wang L V, Single-breath-hold photoacoustic computed tomography of the breast, *Nat Commun*, 9(2018)1–9.

31. Knieling F, Neufert C, Hartmann A, Claussen J, Urich A, Egger C, Vetter M, Fischer S, Pfeifer L, Hagel A, Kielisch C, Multispectral optoacoustic tomography for assessment of Crohn's disease activity, *N Engl J Med*, 376(2017) 1292–1294.

32. Reber J, Willershäuser M, Karlas A, Paul-Yuan K, Diot G, Franz D, Fromme T, Ovsepian S V, Bézière N, Dubikovskaya E, Karampinos D C, Holzapfel C, Hauner H, Klingenspor M, Ntziachristos V, Non-invasive measurement of brown fat metabolism based on optoacoustic imaging of hemoglobin gradients, *Cell Metab*, 27(2018)689–701.

33. Yelleswarapu C S, Kothapalli S R, Nonlinear photoacoustics for measuring the nonlinear optical absorption coefficient, *Opt Express*, 18(2010)9020–9025.

34. OMLC website, http://omlc.org/spectra/index.html.

35. Agrawal S, Suresh T, Garikipati A, Dangi A, Kothapalli S R, Modeling combined ultrasound and photoacoustic imaging: Simulations aiding device development and artificial intelligence, *Photoacoustics*, 24(2021)100304; doi.org/10.1016/j.pacs.2021.100304.

36. Frenette M, Hatamimoslehabadi M, Bellinger-Buckley S, Laoui S, La J, Bag S, Mallidi S, Hasan T, Bouma B, Yelleswarapu C, Rochford J, Shining light on the dark side of imaging: excited state absorption enhancement of a bis-styryl BODIPY photoacoustic contrast agent, *J Am Chem Soc*, 136(2014)15853-15856.

37. Kislyakov I M, Yelleswarapu C S, Nonlinear scattering studies of carbon black suspensions using photoacoustic Z-scan technique, *Appl Phys Lett*, 103(2013)151104; doi.org/10.1063/1.4824448.

38. Yasin A, Nair V S, Aravindh S A, Sarkar SM, Hatamimoslehabadi M, Mitra S, Rahim M H, La J, Roqan I S, Yusoff M M, Yelleswarapu C S, Rajan J, Meso-Zn (ii) porphyrins of tailored functional groups for intensifying the photoacoustic signal, *J Mat Chem C*, 8(2020)8546–8559.

39. Sheik-Bahae M, Said A A, Wei T H, Hagan D J, Van Stryland E W, Sensitive measurement of optical nonlinearities using a single beam, *IEEE J Quant Elect*, 26(1990)760–769.